ECS Transactions, 58 (1) 969-990 (2013)
10.1149/05801.0969ecst ©The Electrochemical Society

# Influence of Platinum Precipitation on Properties and Degradation of Nafion® Membranes

S. Helmly[a,b], B. Ohnmacht[a,b], R. Hiesgen[c], E. Gülzow[a], and K. A. Friedrich[a,b]

[a] Institute of Technical Thermodynamics, German Aerospace Center, Pfaffenwaldring 38-40, 70569 Stuttgart, Germany
[b] Institute for Thermodynamics and Thermal Engineering, University of Stuttgart, Pfaffenwaldring 6, 70550 Stuttgart, Germany
[c] University of Applied Sciences Esslingen, Department of Basic Science, Kanalstrasse 33, 73728 Esslingen, Germany

## Abstract

In this study, the role of Pt concentration and distribution in the membrane on ionomer degradation was investigated. Nafion® membranes were impregnated with different mass fraction of Pt via ion-exchange and operated as membrane electrode assemblies (MEAs) at open circuit voltage (OCV). Various MEAs with known Pt concentration were characterized by electrochemical in-situ measurements regarding both, membrane properties and ionomer degradation. Additionally, Pt particle distribution in the membrane cross sections was analyzed. The presence of Pt precipitations was found to influence ionic conductivity and the sensitivity of cell performance for humidification. Ionomer decomposition increased with concentration and surface area of Pt deposits as well as distance between particles. The comparison between Pt precipitated artificially and during operation showed a considerable difference in particle distribution and extent of internal membrane humidification due to water formation at Pt sites.

## Introduction

A limiting factor for the lifetime of proton exchange membrane fuel cells (PEMFCs) is the degradation of the electrolyte membrane. One of the major causes of degradation is the chemical decomposition of the ionomer due to radicals which are formed at Pt precipitation in the membrane (1). Pt precipitates in the membrane as follows: Metallic Pt dissolves to Pt ions at the cathode due to the high electrode potential. Consequently, Pt ions are transported into the membrane where they are reduced again to metallic Pt by the permeating hydrogen (2, 3). These Pt precipitations now serve as catalytic sites where hydrogen peroxide, formed at the electrodes, decompose to hydroxyl radicals, which can attack the ionomer (1).

Ionomer degradation in the presence of Pt deposit was verified based on membrane thinning and traces of polymer in the condensate water (4-6). The examination of the membrane with further analysis methods such as micro Raman spectroscopy and Fourier

transform IR spectroscopy gave further evidence (7, 8). Moreover, fluoride emission was found to correlate with the amount of Pt deposited inside the membrane (4, 9).

The influence was also studied with artificially Pt impregnated membranes. Those experiments showed contradictory results. On the one the hand side, large ionomer defects, weight loss and high fluoride emission rate (FER), as well as an increased radical formation, for aged Pt-impregnated membranes was reported (10, 11). On the other hand, less FER was observed for Pt-impregnated membranes than for conventional membranes (12, 13). The authors assumed that hydrogen peroxide or radicals were easily scavenged by Pt precipitations. Gummalla et al. explained these different results by the Pt loading (14). They noted that, depending on particle size and concentration, OH radicals are either directly scavenged by Pt or are able to attack the polymer. In a recent study this theory is addressed. In a degradation test, Rodgers et al. studied the degradation of Pt impregnated membranes with varying Pt concentration of 10, 30 and 50 mol-% Pt (15). Since no electrodes were applied to the membrane, additional Pt precipitations originating from the electrode were prevented. Their results showed a strong effect of Pt concentration on membrane degradation. Fluoride emission was significantly enhanced with 10 mol-% Pt compared to a non impregnated membrane, whereas 30 and 50 mol-% resulted in a reduced degradation. They concluded that the increased degradation in case of the 10 mol-% Pt is caused by the higher concentration of smaller Pt particles, as TEM analysis showed.

The aim of this paper is to further investigate the role of concentration and distribution of Pt precipitation in the membrane for ionomer degradation. For the first time, our study adds electrochemical characterization to the examination of degradation and particle distribution of artificially Pt impregnated membranes with different Pt fraction. For this purpose, Nafion® membranes were impregnated with Pt via ion-exchange. To prevent additional deposition of Pt in the ionomer during the subsequent degradation test of ~140 h at OCV, Pt-impregnated membranes were coated with electrodes, which exhibited high Pt stability. The MEAs were characterized by electrochemical in-situ measurements such as polarization curve, impedance spectroscopy and cyclic voltammetry. Ionomer degradation was further measured by means of FER. Additionally, scanning electron microscopy (SEM) and energy-dispersive X-ray (EDX) spectroscopy were used to analyze Pt particle distribution in the membrane cross sections. For comparison of Pt precipitated artificially and during operation, a MEA with electrodes exhibiting a higher Pt solubility was also tested.

## Experimental

### Preparation and Operation of MEAs

MEAs with Nafion® N212 membranes were used in all experiments. For the fabrication of Pt-MEAs, Nafion® NRE-212CS membranes (DuPont) were impregnated. The commercially available catalyst coated NR-212 membrane (Ion Power) was used for comparison. It has to be noted that according to the manufacturer, both membrane types are chemically stabilized.

Impregnation of Membranes with Pt. Platinum was dispersed in the NRE-212CS membranes based on the impregnation-reduction method described by Fedkiw (16). First, a membrane sheet of around 7 cm x 7 cm in $H^+$ form was treated for 24 h in 500 ml 1.0 M NaCl solution at room temperature to exchange it to $Na^+$ form. This enhances the subsequent Pt ion-exchange and prevents esterification of pentanol (17, 18). Then, the membrane was rinsed for 1 h in 200 ml de-ionized water at room temperature and dried with filter paper. To transfer it into $Pt^{2+}$ form, the membrane was equilibrated for 24 h in 200 ml $[Pt(NH_3)_4]Cl_2$ (Sigma Aldrich) aqueous solution at $T_{Pt,\ ex}$ = 60 - 80 °C. The Pt concentration of the solution was varied from 0 to 254 $mg_{Pt}\ l^{-1}$ to obtain different Pt content in the membranes. After this, the membrane was again rinsed for 1 h in 200 ml de-ionized water at room temperature and dried with filter paper. In the reduction step, $Pt^{2+}$ ions were reduced to metallic Pt by stirring for 2 h at $T_{Pt,\ red}$ = 125 °C in 100 ml 1-pentanol (Merck) and with one exception at 60 °C in ethanol. After impregnation, the membrane was exposed for 2 h to a 200 ml 0.5 M $H_2SO_4$ solution (Merck) at room temperature to exchange it again into $H^+$ form. Finally, the membrane was rinsed for 2 h in 200 ml de-ionized water at room temperature.

For determination of the Pt content, membranes were dried for 24 h at 80 °C and weighed, before and after the impregnation treatment. According to this, membranes had a Pt content from 0 to 46 mg-Pt $g^{-1}$-Nafion® in their BOT state.

MEA Fabrication. After impregnation, membranes were coated with electrodes at an area of 23 cm² using the DLR dry-spraying method (19). The catalytic layer consisted of Pt black and 30 wt-% Nafion® ionomer powder. The ionomer powder used in the dry spraying technique is produced by freeze milling Nafion® resin NR-50 (DuPont). The Pt loading was 0.2 $mg_{Pt}\ cm^{-2}$ at the anode, respectively 0.4 $mg_{Pt}\ cm^{-2}$ at the cathode. Finally, the catalyst coated membranes were placed between gas diffusion layers (Sigracet SGL-BC25) and hot-pressed for 3 min at 160 °C under a pressure of 690 N $cm^{-2}$. The reference membrane (NR-212) was obtained with a Pt/C coating (0.3 $mg_{Pt}\ cm^{-2}$) at an area of 25 cm² on both sides. It was also sandwiched between gas diffusion layers and hot pressed as described above. Table I lists all MEAs examined in this work. Due to MEA failure, not all of them could be tested in the degradation experiment and analyzed at the end of the test (EOT). Still, they were all examined by means of SEM/EDX at the beginning of the test (BOT).

**Table I. List of examined MEAs.**

| Pt concentration / mg-Pt $g^{-1}$-Nafion | Remark | MEA | $T_{Pt, red}$ / °C | $T_{Pt, ex}$ / °C |
|---|---|---|---|---|
| 0 | | Ion Power NR-212 | - | - |
| 0 | | NRE-212CS | - | - |
| 0 | Not tested | NRE-212CS | - | - |
| 0 | Not tested | NRE-212CS | 125 | 80 |
| 6.4 | | NRE-212CS | 60 (ethanol) | 80 |
| 12.3 | | NRE-212CS | 125 | 60 |
| 18.4 | | NRE-212CS | 125 | 80 |
| 27.3 | Not tested | NRE-212CS | 125 | 70 |
| 32.6 | | NRE-212CS | 125 | 70 |
| 34.5 | | NRE-212CS | 125 | 80 |
| 36.3 | Tested 575 h | NRE-212CS | 125 | 60 |
| 46.5 | 150 % r.H. | NRE-212CS | 125 | 80 |

Test Procedure. The prepared MEAs were tested as single cells using plates with single serpentine flow fields. The cell plates were bolted together applying a tightening torque of 6 Nm. Humidifiers with control of humidification level through adjustment of dew point temperature were used for gas humidification. In all experiments, the cell was fed with gases under atmospheric pressure. Before the actual degradation experiment, each cell was conditioned as follows: the cell was fed with saturated hydrogen on the anode side and saturated air on the cathode with flow rates of 120 respectively 400 sccm at a cell temperature of 80 °C and at a constant cell voltage of 500 mV. When the cell current exceeded 0.5 A $cm^{-2}$ the electronic load was switched to galvanostatic mode at a current density of 0.5 A $cm^{-2}$ for ca. 24 h to reach steady state. After the initial conditioning, the MEAs were characterized by means of polarization curve, cyclic voltammetry (CV) and electrochemical impedance spectroscopy (EIS). In the degradation test, the MEAs were operated for ca. 140 h under OCV conditions. The cell temperature was set to 80 °C. Air and hydrogen were fed to the cells with flow rates of 60, respectively 15 sccm, at 80 °C under ambient pressure. During the degradation test, condensate water from anode and cathode side was collected in polyethylene bottles for analysis of fluoride emission. Subsequent to the degradation test, MEAs were again electrochemically characterized.

MEA Characterization

Cell Performance. Polarization curves were performed in potentiostatic mode with the cell temperature set to 80 °C. To control the humidification level, humidifiers with adjustment of dew point temperature were used. Since test benches allowed no lambda control, flow rates were set to 360, respectively 1200 sccm, during the entire measurement corresponding to the current density of 1.5 A $cm^{-2}$ at a hydrogen/air stoichiometry of 1.5/2.0. Gas pressures could not be directly controlled but were regulated by the atmospheric pressure at the cell outlet, which resulted in an absolute

pressure at the cell inlet of around 1200 mbar at the anode, respectively 1700 mbar at the cathode. Each operation point was held for at least 2 minutes.

Electrical Conductivity of the Cell. For calculating the electrical conductivity of the cell $\sigma = d / (A \cdot R_{el})$, electrical resistance $R_{el}$ and membrane thickness d have to be measured in addition to the known geometric area of the electrode A. The membrane thickness was determined based on micrographs, as described in a later section.

$R_{el}$ was measured using EIS. The measurements were carried out with the electrochemical workstation IM6 in combination with the potentiostat PP241 (Zahner Elektrik). They were recorded in galvanostatic mode in the frequency range from 50 mHz to 100 kHz at a current density of 0.5 A $cm^{-2}$ with an amplitude of 10 mV. Gas flow rates were 120 sccm on the anode and 400 sccm on the cathode side. In order to achieve steady state, the cell was pre-polarized at least 15 min prior to the start of the EIS measurement at the same current density set during EIS.

Cell resistances were determined fitting the experimental data to an equivalent circuit using the software Thales Z2.15. The equivalent electrical circuit used within the simulation is shown in Figure1. In this model, $R_{el}$ is represented by an ohmic resistance. It contains the electrical contact resistance of the cell, as well as the ionic and electronic resistance of the membrane (20). In fuel cell membranes, the electronic resistance is normally negligible compared to its ionic resistance. The kinetic of anode and cathode as well as the mass transfer (combined for both electrodes) are each represented by an ohmic resistance connected parallel to a capacitance. The latter is described by a constant phase element. Furthermore, the wiring of the measurement equipment is considered by the inductive resistance L.

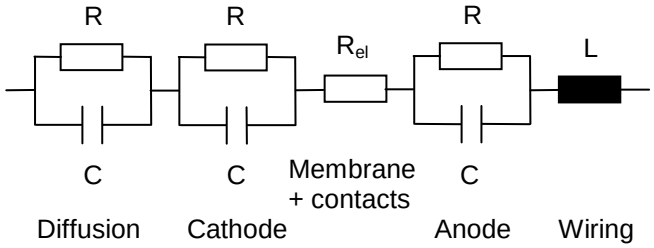


Figure1. Equivalent circuit for analysis of EIS data

Hydrogen Permeation. The permeation of hydrogen through the membrane was measured by means of cyclic voltammetry. The measurements were carried out with the electrochemical workstation IM6 in combination with the potentiostat PP241 (Zahner Elektrik). CV was performed with hydrogen on the anode side and nitrogen on the cathode side. The humidified gases were fed at 80 °C with $H_2/N_2$ flow rates of 50/20 sccm at a cell temperature of 80 °C. Prior to the measurement, the cell was conditioned for 30 min. Then, the cathode was cycled five times between 60 and 550 mV at a scan rate of 40 mV $s^{-1}$. Hydrogen crossover was calculated based on the data of the last cycle after subtracting the double layer charge in the voltammogram.

Fluoride Emission. Fluoride ion concentration in the collected anode and cathode condensate was measured using an ion selective electrode (laboratory meter ProLab 4000

and fluoride electrode F 60, SCHOTT Instruments), which was calibrated over the range of 10-10000 $\mu mol_F\ l^{-1}$ using KF aqueous standard solutions. Standard samples and 15 ml of condensate samples were diluted with buffer solution (TISAB II, Bernd Kraft GmbH) 1:1. The reading of the meter was recorded after equilibrium was reached; typically 5-10 min after the electrode was immersed into the solution.

Examination of Membrane Cross Sections. Membrane cross sections were examined by means of SEM and EDX regarding membrane thickness and distribution of Pt particles. Samples with a width, i.e. length of cross-section, of around 3 mm were cut from the MEAs before and after the operation in the test station. The samples taken before the test were cut from the uncoated membrane fringe, the samples after the test from the active area of the cell. Particle distribution was analyzed on a sample of the center of the cell. Membrane thickness was additionally measured on samples of the gas inlet and outlet area. For preparation of cross-sections via freeze-fractioning, GDLs were removed from the samples which were then immersed in liquid nitrogen and broken.

SEM and EDX measurements were conducted on an ULTRA plus (Zeiss Corp.) scanning electron microscope. The images were recorded based on secondary electrons (SE) and backscattered electrons (BE). The resolution of the microscope was 1.0 nm at 15 kV and 1.7 nm at 1 kV. For SE images, the voltage was set to 5 kV; for BE images, it was set to 5 kV or 10 kV. The SEM was equipped with an XFlash® 5010 EDX detector (Bruker Corp.) that has an energy resolution of 123 eV at Mn Kα. EDX measurements were performed for 180 s at 10 kV. The sensitivity limit of the elemental detection was approximately 0.1 %. Each cross section was investigated at three different positions. At each position, EDX line scans with a spacing of 0.1 µm were recorded to determine the Pt distribution along the membrane thickness. For a detailed investigation of Pt particle distribution, micrographs (ca. 0.8 µm x 0.6 µm) of the membrane section near anode, cathode and membrane center were recorded. Furthermore, SEM images were used to determine the thicknesses of the membranes. Each presented thickness value is the average value of at least nine measurements conducted on random spots on the sample. SEM micrographs were analyzed with the software ImageJ 1.46r (National Institute of Health) to determine position and size of single particles. Based on this data, particle density, particle intensity, nearest neighbor distance and normal distribution of particle size was calculated to describe the particle pattern.

To verify SEM/EDX data, the MEA with 6.4 mg-Pt $g^{-1}$-Nafion® was also measured regarding the presence of Pt in the membrane by means of X-ray diffraction (XRD). X-ray diffractograms were recorded with a D8 Discover X-ray diffractometer (Bruker Corp.) equipped with a VÅNTEC-2000 area detector. Exposures were made in reflection mode with a tuned monochromatic and parallel X-ray beam (Cu-Kα). The accelerating voltage was 45 kV and the tube current was 0.650 mA. Each diffraction pattern was measured in four frames with a step size of 23 °, starting with $\Theta_1 = \Theta_2 = 12$ ° (Bragg-Brentano condition) and a exposure time of 180 s/frame. For the determination of the mean Pt crystallite size, diffractograms were analyzed by means of the Rietveld refinement method using the software Diffracplus Topas (Bruker Corp.).

## Results and Discussion

Distribution of Pt in Membrane

Non-impregnated Membrane. To clarify the influence of the in-house electrodes as a possible source for Pt deposits in the membrane, cross sections of a non-impregnated membrane in BOT and EOT condition were analyzed for Pt by means of EDX. The measured Pt profile along the membrane thickness is shown in Figure 2. Besides the two peaks of the electrodes below 0 µm and above ~50 µm, Pt was neither detected in the BOT nor in the EOT membrane sample. In contrast, the presence of Pt was distinctly verified in the Pt-impregnated membranes shown in Figure 4. It follows that the in-house applied electrodes showed a high Pt stability and can be neglected as a source for Pt deposits. Thus, Pt content in the impregnated membranes originated only from the impregnation procedure.

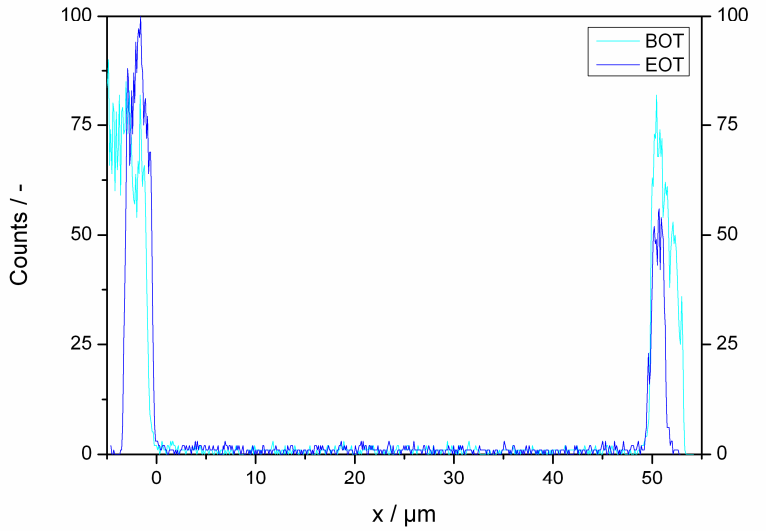


Figure 2. Pt profile across the MEA with a non-impregnated membrane and in-house applied electrodes before and after the degradation test. Data were measured by means of EDX line scans. The anode is at x < 0 µm, the cathode is represented by the large peak on the right side of the scan.

Pt-impregnated Membranes. Pt deposition in Pt-impregnated membranes was examined on samples in BOT and EOT condition. In the BOT condition, Pt precipitation in the membranes could not be detected in SEM micrographs and in the XRD diffractogram in Figure 3. However, EDX measurements clearly proved the presence of Pt as can be seen in the Pt profile across a Pt-impregnated membrane in Figure 4. The fact that the counts for the BOT sample are higher than for the EOT sample does not necessarily imply a difference in Pt concentration. This could be attributed to the influence of the fractured surface. In the EOT condition, Pt particles were clearly visible in micrographs (Figure 5) and also noticeable as peaks in the diffractogram. This indicates that deposited Pt particles were initially smaller than the detection limit of around 4 nm and grew during the experiment. As a consequence, analysis of particle distribution in this study is limited to the EOT membranes due to the limits of XRD and SEM.

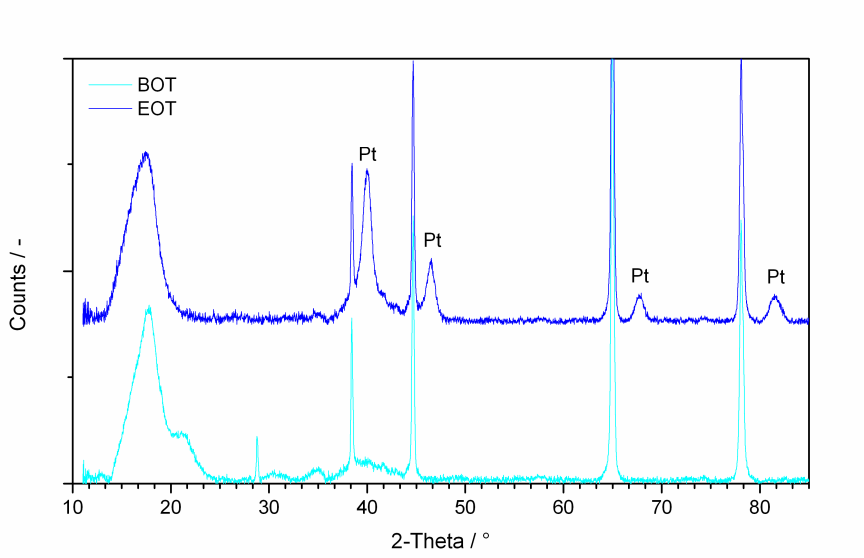


Figure 3. XRD diffractogram of the MEA with 6.4 mg-Pt $g^{-1}$-Nafion® before and after the degradation test.

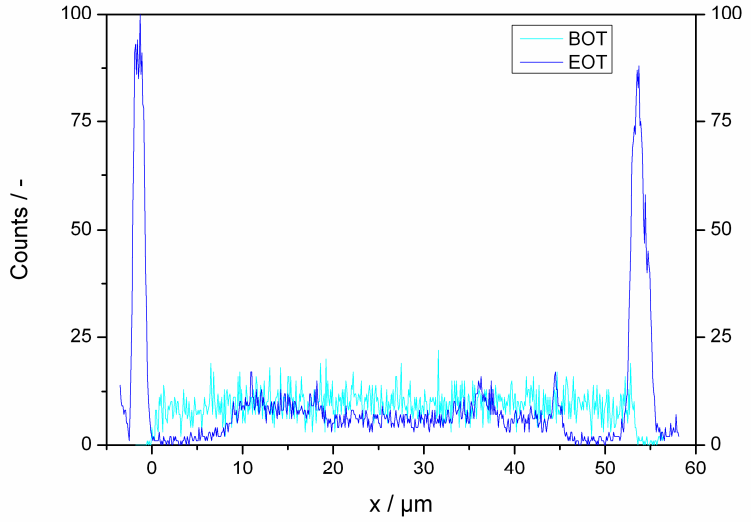


Figure 4. Pt profile across the Pt-MEA with 32.6 mg-Pt $g^{-1}$-Nafion® before and after the degradation test. Data were measured by means of EDX line scans. The anode is at $x < 0$ µm, the cathode is represented by the large peak on the right side of the scan.

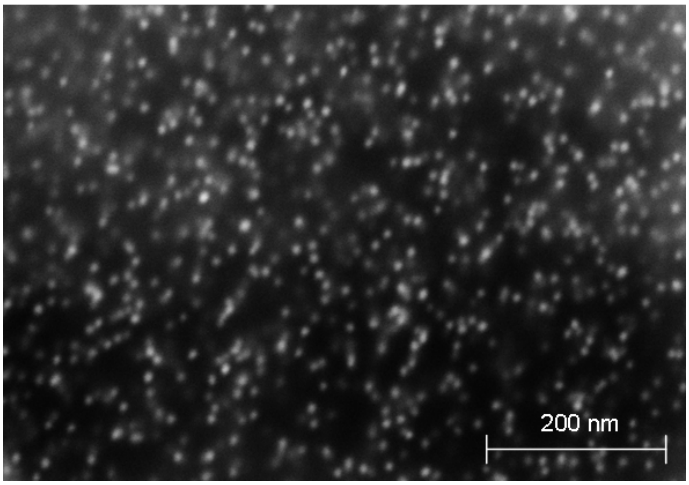


Figure 5. SEM micrograph of Pt precipitations in the Pt-impregnated membrane with 32.6 mg-Pt $g^{-1}$-Nafion® after the test.

The Pt profile in Figure 4 also reveals that the Pt distribution is almost homogeneous after the impregnation but changes are induced during the operation. Considering further line scans of EOT samples (Figure 6), it becomes obvious that Pt concentration dropped in the proximity of the cathode but increased in the central area of the membrane. This redistribution is most probably caused by the high tendency of small nucleates to redissolve and by the migration of positively charged ions towards the negative anode in the electric field under current flow. As a consequence, Pt precipitations near the cathode are dissolved again and transported further into the membrane where they redeposit. It can also be seen, that Pt peaks became more distinct for membranes which had a higher Pt concentration or which were tested longer. In fact, the longer test duration led to loss of membrane thickness as the different lengths of the line scans indicate. Therefore, assuming Pt was not lost, Pt concentration was indirectly raised. The increased concentration at certain locations could have been caused by local conditions like gas concentration which facilitated growth respectively deposition of Pt particles and/or ionomer degradation (21).

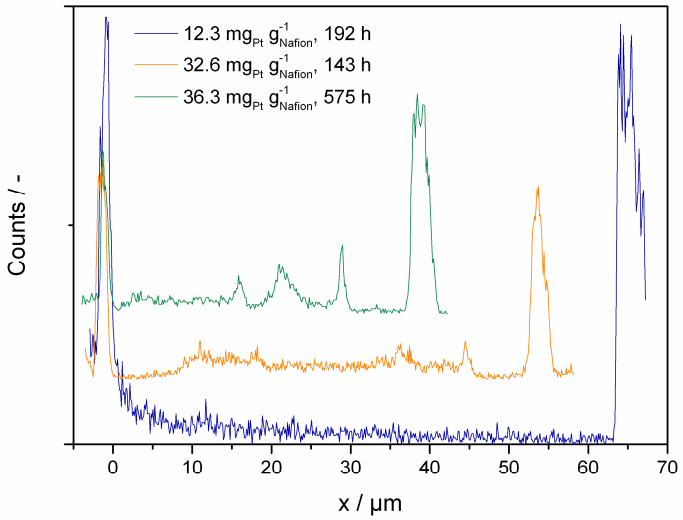


Figure 6. Pt profiles across Pt-MEAs with different Pt concentration after the degradation test. Data were measured by means of EDX line scans. The anode is at x < 0 µm, the cathode is represented by the large peak on the right side of the scan.

Taking into account the heterogeneous Pt profile, the analysis of the particle distribution presented in the following is constricted to the area of the membrane centre.

Figure 7 shows the particle intensity, i.e. number of Pt particles per area, plotted against the Pt concentration. It can be seen, that the intensity increased linearly with the amount of Pt in the membrane. Only the MEA with 18.4 mg-Pt $g^{-1}$-Nafion® apparently represents a runaway value of 2.8 x $10^{-3}$ particles per $nm^2$ which was considered in the analysis.

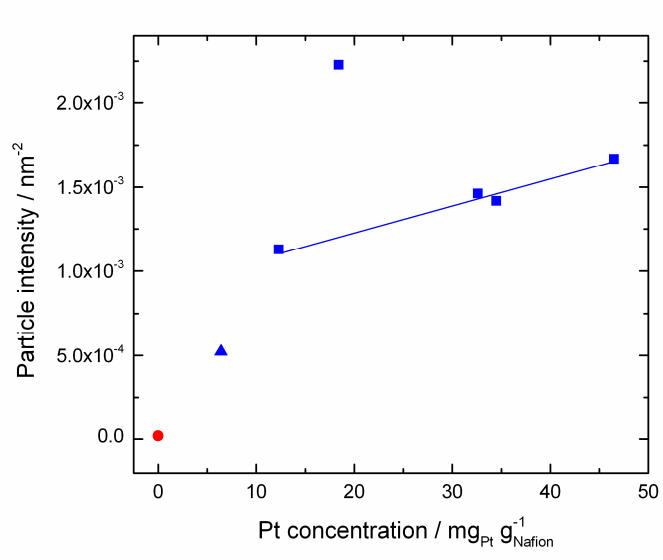


Figure 7. Result of Pt distribution analysis in the centre of the membranes: particle intensity of the reference MEA (●), Pt-MEAs reduced with 1-pentanol at $T_{Pt, red}$ = 120 °C (■) and reduced with ethanol at $T_{Pt, red}$ = 60 °C (▲).

Such a strong dependence on Pt concentration can not be seen in the average particle diameter and the average nearest neighbor distance in Figure 8. The sample with 6.4 mg-Pt $g^{-1}$-Nafion®, which is the only membrane in the test where Pt-ions were reduced with ethanol and at $T_{Pt,\ red}$ = 60 °C, exhibits the highest values of (9.4 ± 1.7) nm particle diameter and 26.3 nm nearest neighbor distance. For this sample, additional XRD measurements were conducted. Based on this data, the average size of Pt crystallite in the EOT sample was determined to be 9.4 nm which corresponds to the SEM data for particle size and therefore give evidence for crystallite growth being the dominant particle growth mechanism in the Pt-impregnated membranes.

The membranes with 1-pentanol as reducing agent and $T_{Pt,\ red}$ = 120 °C show lower values for density and intensity as well as the tendency of an increased diameter with Pt concentration, ranging from (5.6 ± 1.0) nm to (8.1 ± 1.8) nm. A significant influence of the Pt amount on the average distance can not be seen.

The increasing standard deviation of the average diameter wit Pt concentration reveals that the particle size tends to be distributed more broadly with increased Pt amount. Furthermore, it becomes evident that distribution of low Pt concentration at $T_{Pt,\ red}$ = 60 °C with ethanol is similar to high Pt concentration at $T_{Pt,\ red}$ = 120 °C with 1-pentanol.

To sum up the findings, an increase in Pt concentration leads to a higher concentration of larger particles without significantly affecting their average minimum distance to each other.

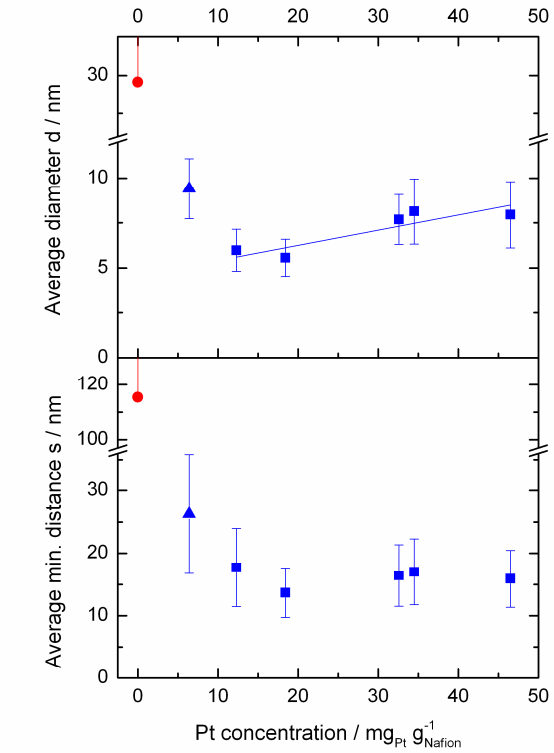


Figure 8. Result of Pt distribution analysis in centre of membranes: average diameter and minimum nearest neighbor distance of the reference MEA (●), Pt-MEAs reduced with 1-pentanol at $T_{Pt,\ red}$ = 120 °C (■) and reduced with ethanol at $T_{Pt,\ red}$ = 60 °C (▲).

Reference Membrane. A comparison of Pt precipitated artificially and during operation, is enabled by the data of the Ion Power MEA. Figure 9 shows the Pt profile in the EDX line scan across this MEA after the test. A single peak appears at ~34 µm and represents the location of the Pt band. This is the only area, where particles are visible in SEM images.

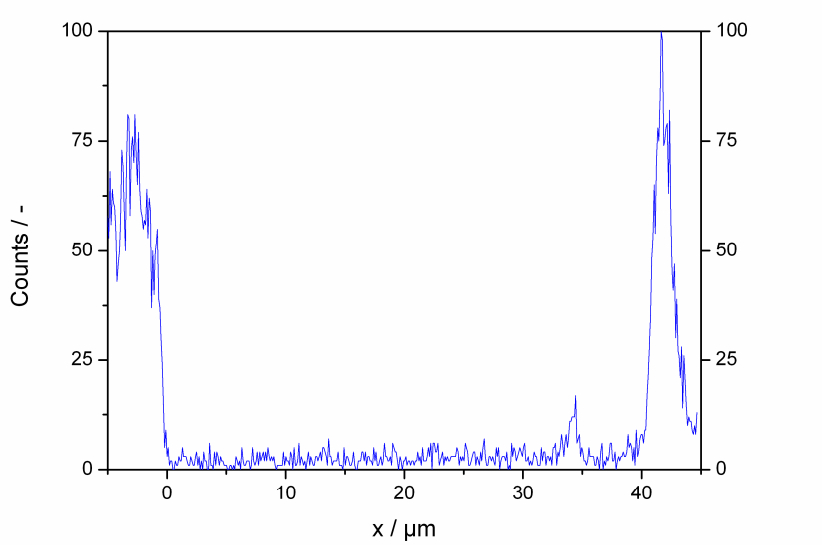


Figure 9. Pt profile across the reference MEA after the degradation test at EOT. Data was measured by means of EDX line scans. The anode is at x < 0 µm, the cathode is represented by the large peak on the right side of the scan.

From the micrograph in Figure 10, it is apparent that the particles in this band differed considerably from the ones deposited by impregnation (see Figure 5). The data of the particle distribution in Figure 7 and Figure 8 reflect this clearly: intensity and density of particles is by far lower. In contrast, the average particle has a diameter of 29.1 nm and is substantially larger than the ones in the Pt membranes, which are smaller than 10 nm. The size of the particles and their big average distance of 115.4 nm suggest that particles were growing to a much larger extent when precipitating during fuel cell operation. Considering the relatively high standard deviation of the diameter of 14.2 nm, it can be concluded that the growth was strongly irregular.

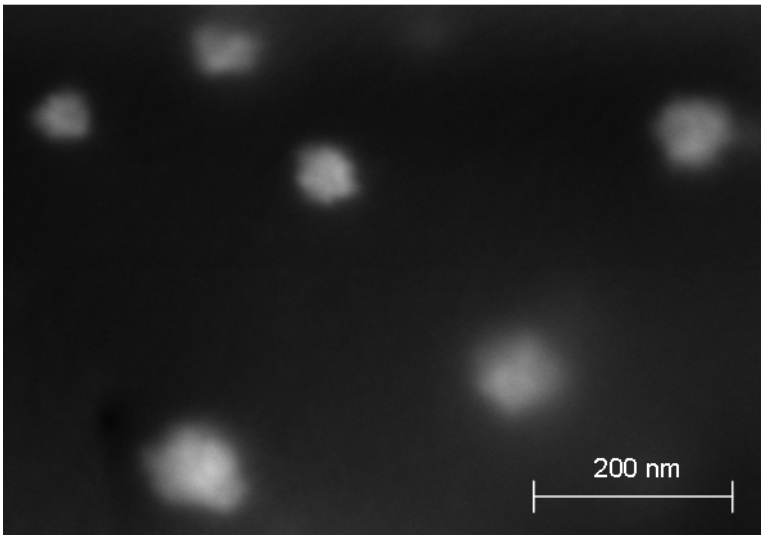


Figure 10. SEM micrograph of Pt precipitations in the membrane of the reference MEA at EOT.

A possible explanation for this difference in particle distribution is the dependence of Pt solubility on particle size (22). The higher solubility of the Ion Power cathode led to a steady supply of mobile Pt ions or small Pt particles which deposited on already existing Pt particles in the membrane. As a consequence, their growth was only limited by the available supply. In contrast, the cathode of the Pt-impregnated membranes did not provide any Pt ions due to their higher stability. Thus, the initial growth of these Pt particles stopped when particles reached a certain diameter, which led to immobility and increased stability of the smaller particles.

Influence of Pt Precipitation on MEA Properties

Figure 11 shows polarization curves at various levels of gas humidification for three Pt-impregnated membranes with different Pt concentration. The plots clearly demonstrate that sensitivity to humidity is influenced by Pt: the higher the amount of Pt, the higher the drop of cell current at lower humidification. It is notable, that the change in humidification mainly affects the linear section in the polarization curves. Thus, the loss in performance can be attributed to an increased ohmic cell resistance, as reported by Lee et al. (23).

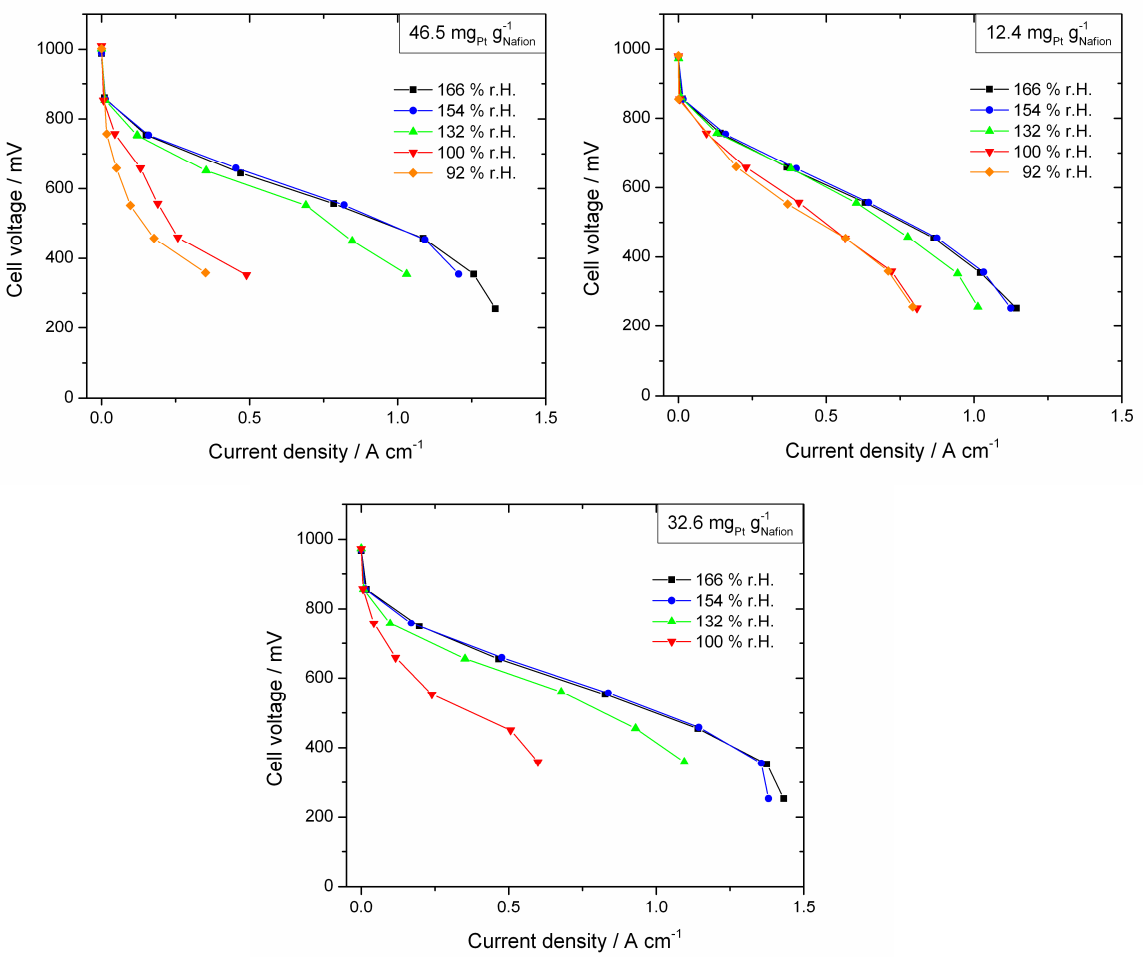


Figure 11. Polarization curves at various levels of gas humidification for three Pt-impregnated membranes with different Pt concentration at BOT. Cell temperature was set to 80 °C, flow rates to 360/1200 sccm hydrogen/air with gas pressures (abs.) at inlet of anode/cathode of 1200/1700 mbar.

This is confirmed by the electrical conductivity plot shown in Figure 12. The data were recorded at 100 % r.H. and its decrease thus reflects the drop of electrical conductivity with increasing Pt concentration at non-oversaturated humidification.

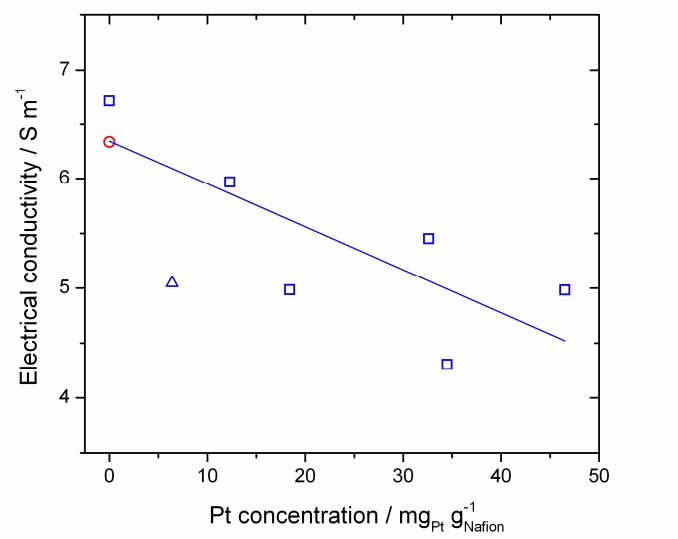


Figure 12. Electrical conductivity of the reference MEA (○), Pt-MEAs reduced with 1-pentanol at $T_{Pt,\ red}$ = 120 °C (□) and reduced with ethanol at $T_{Pt,\ red}$ = 60 °C (△) at BOT.

The electrical cell resistance includes contact resistances of the cell, as well as the ionic and electronic resistance of the membrane. Taking the observed influence of humidification into account, it can be concluded that the change of electrical conductivity was caused by the ionic resistance of the membrane. Less clear is the relation between $H_2$ permeability and Pt concentration shown in Figure 13. The slight increase of $H_2$ flux could be interpreted as a correlation with Pt concentration. But the big difference of the MEA with 34.5 and 46.5 mg-Pt $g^{-1}$-Nafion, do not support this assumption. Still, it can be concluded that proton transport is unambiguously decreased by Pt concentration, whereas gas permeation is not. This indicates that Pt precipitations mainly block ionic paths in the membrane.

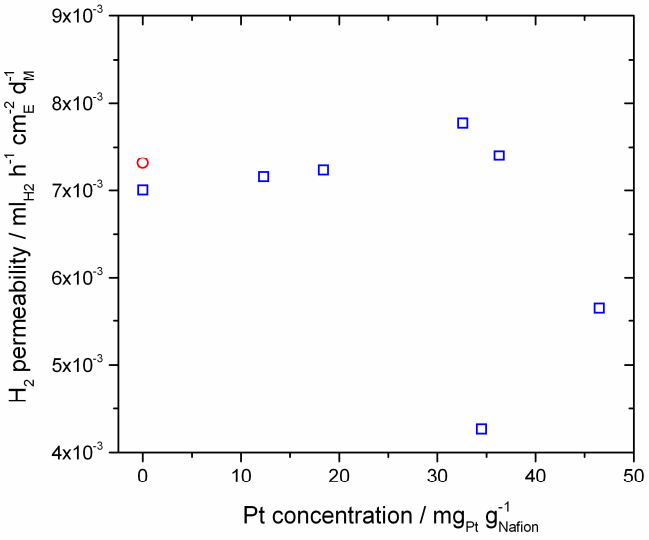


Figure 13. $H_2$ permeability of the reference MEA (○) and Pt-MEAs reduced with 1-pentanol at $T_{Pt,\ red}$ = 120 °C (□) at BOT. Values are normalized with respect to test duration, electrode area and membrane thickness.

In some studies, impregnation with Pt was used for self humidification of the membrane since hydrogen and oxygen react to water at the catalytic sites (17, 23, 24). It was reported that this improves the cell performance at low relative humidity (17). Our results do not indicate the occurrence of this effect at BOT, since this would imply an increase of ionic conductivity, gas permeation and should also reduce sensitivity to humidification (24, 25).

## Result of Degradation Test

Membrane Thickness. An indicator for ionomer degradation is the loss of membrane thickness. Figure 14 shows this data for cells tested in the degradation experiment. Whereas the in-situ precipitation clearly led to membrane thinning, Pt-impregnated membranes surprisingly increased in thickness with the exception of the one with ethanol as reducing agent and the MEA operated for 575 h. Unfortunately, we cannot clarify if swelling was accompanied by shrinkage in membrane area since membrane sheets were cut by hand and varied in area within a few millimeters. In our opinion, the most probable explanation for the increase is significant swelling of the Pt-impregnated membranes due to water uptake during the degradation test. The dependence on Pt concentration indicates that this was caused by self humidification. Since the cells were operated at OCV, $H_2$ and $O_2$ were not consumed at the electrodes and could diffuse through the membrane, where they combined at Pt deposits to water. A possible reason why this effect was not observed at BOT, could be the short duration of operation before BOT measurements and the operation conditions with low crossover fluxes of the reactants. But for interpretation of EOT data, self humidification has to be taken into account.

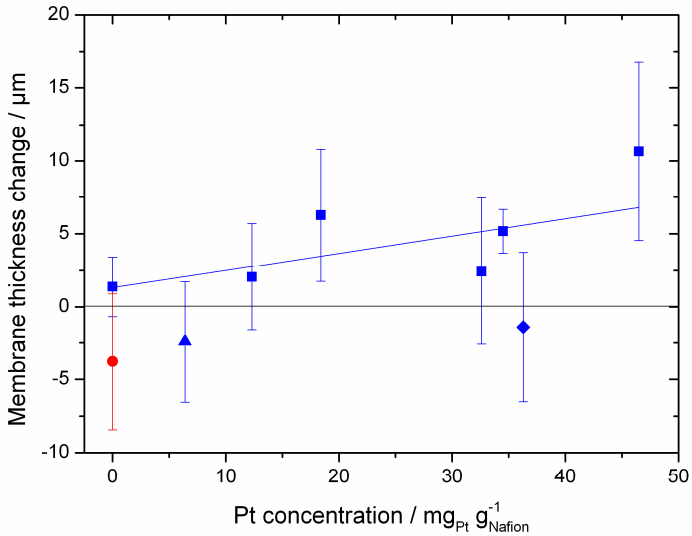


Figure 14. Change of membrane thickness during the degradation test for the reference MEA (●), Pt-MEAs reduced with 1-pentanol at $T_{Pt,\ red}$ = 120 °C (■) and reduced with ethanol at $T_{Pt,\ red}$ = 60 °C (▲), as well as of the Pt MEA operated for 575 h (◆).

In the case of the Pt-impregnated membrane reduced with Ethanol and the one operated longer, the decrease of membrane thickness can be associated with a high ionomer loss, as the FER in Figure 15 (respectively the calculated total fluoride emission) demonstrates. This means that the decrease in thickness due to membrane decomposition exceeded the swelling induced increase. The reference membrane also exhibited distinct

membrane thinning. Although its Pt concentration was not determined quantitatively, the conclusion can be drawn from the comparison of EDX data in Figure 4 and Figure 9 that its Pt mass fraction is considerably lower than in the Pt-impregnated membranes. Swelling in the reference membrane due to internal humidification is therefore unlikely.

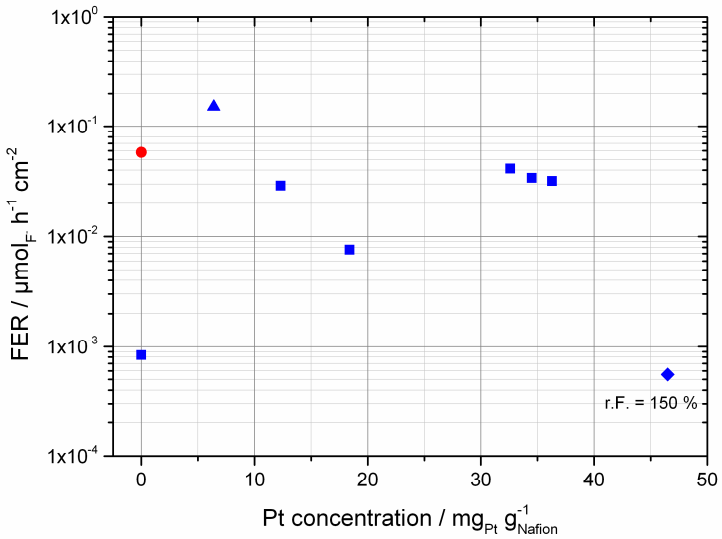


Figure 15. Fluoride emission detected in the condensate of the reference MEA (●), Pt-MEAs reduced with 1-pentanol at $T_{Pt, red}$ = 120 °C (■) and reduced with ethanol at $T_{Pt, red}$ = 60 °C (▲) as well as of the Pt-MEA operated at 150 % r.H. (◆). FER is normalized with respect to test duration and active area.

Because of the additional influence of membrane swelling for Pt-impregnated membranes, change in membrane thickness is not a representative measure for evaluating ionomer degradation. More suitable is the FER shown in Figure 15. A direct relation to Pt concentration is not evident. But the comparison with Figure 8 reveals a correlation with the diameter, respectively surface area, and the minimum distance of particles, which is demonstrated in Figure 16. This finding is in contrast to the result reported by Rodgers et al. (15). Whereas we found an increase of FER with increasing concentration and size of particles, they reported increased degradation for small particles. The most plausible explanation for this is the difference in Pt concentration. They were investigating membranes with 0, 10, 30 and 50 mol-%, respectively 0, 17.9, 53.6 and 89.3 mg-Pt $g^{-1}$-Nafion® and found substantially reduced FER for the two MEAs with the highest Pt content. Apparently, chemical decomposition is suppressed at this high Pt fraction due to quenching of radicals.

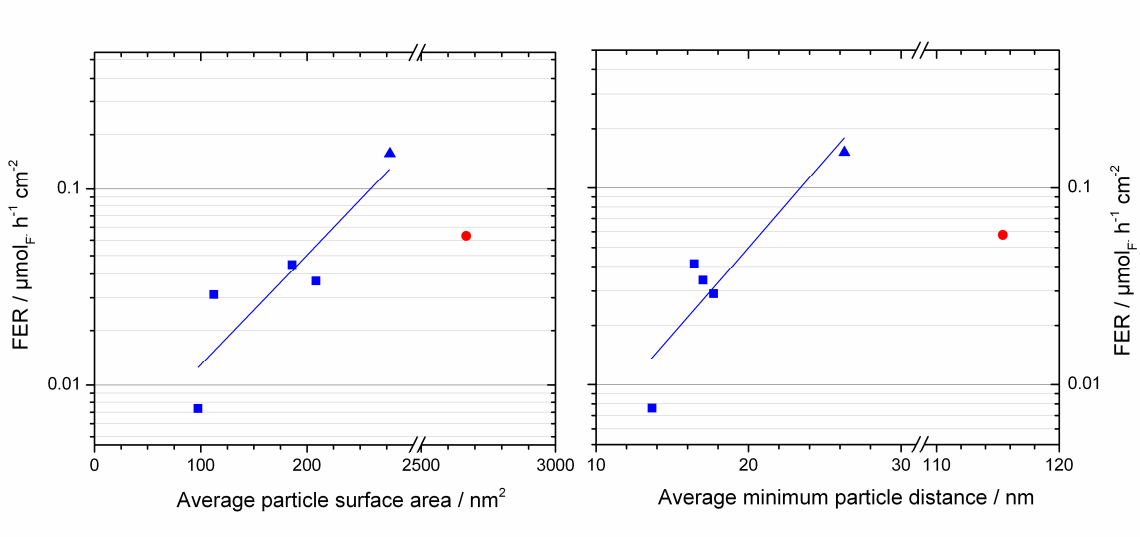


Figure 16. Average surface area and minimum distance of particle distribution in dependence on FER of the reference MEA (●), Pt-MEAs reduced with 1-pentanol at $T_{Pt, red}$ = 120 °C (■) and reduced with ethanol at $T_{Pt, red}$ = 60 °C (▲). FER is normalized with respect to test duration and active area.

Only the Pt-impregnated membrane operated with gas humidification of 150 % (46.5 mg-Pt $g^{-1}$-Nafion®) did not show this relation. It had an even lower FER than the treated membrane with 0 mg-Pt $g^{-1}$-Nafion®, which means that the increase of humidification was suppressing ionomer degradation. Since the water uptake of this high loaded Pt-impregnated membrane was already significantly increased due to the internal humidification, it can be assumed that the increase in gas humidification mainly affected the electrodes. The excess water might have led to flooding so that the formation of $H_2O_2$ at the electrodes and diffusion of $H_2$ and air into the membrane were reduced considerably. As a consequence, chemical decomposition of the ionomer was constrained.

The reference membrane exhibited the second highest FER. But regarding the dependence on surface area and distance as found for the Pt-impregnated membranes, its large particles with big distances to each other should result in a substantially higher FER. This assumption fails however to capture the difference in Pt concentration. As mentioned before, Pt precipitations in the Ion Power membrane were found to be distributed in a narrow Pt band and not throughout the whole cross section. Thus, the total active surface of the Pt precipitations is smaller and therefore also a local chemical decomposition of the ionomer is expected.

Hydrogen Permeability. According to Fick's first law, diffusion flux is the product of diffusion coefficient and concentration gradient. Since water uptake, Pt precipitations and membrane thickness are changing during the test, influencing both parameters, the data of hydrogen permeability must be interpreted with caution. But the strong influence of swelling can be eliminated by normalizing the $H_2$ crossover flux with respect to the membrane thickness at BOT respectively EOT, as can be seen in Figure 17. This data illustrates the influence of change in diffusion coefficient during the degradation test.

Apparently, the value at 32.6 mg-Pt $g^{-1}$-Nafion® represents a runaway value, so that there is the tendency of a slight permeability reduction with increasing Pt concentration for the Pt-impregnated membranes. The increased water uptake of the membrane cannot explain this result, since humidification improves permeability (25). This suggests that the suppression of the $H_2$ flux due to reaction at Pt precipitations was enhanced.

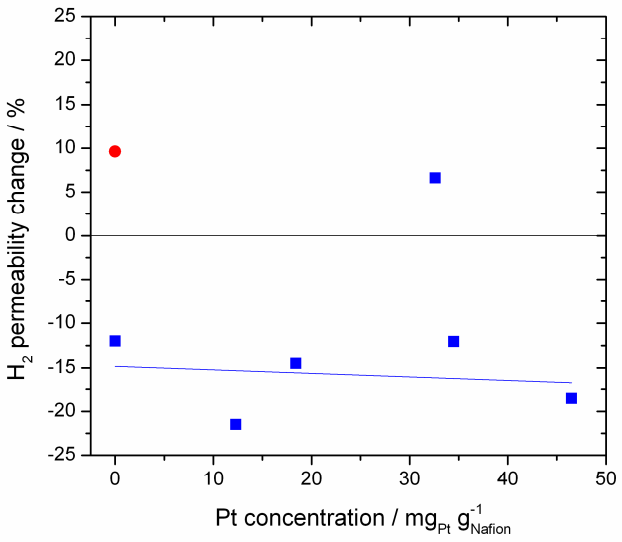


Figure 17. Change of $H_2$ permeability of the reference MEA (●) and Pt-MEAs reduced with 1-pentanol at $T_{Pt, red}$ = 120 °C (■) during the degradation test. Values of permeability were normalized with respect to membrane thickness.

In contrast to the Pt-impregnated membranes, the reference membrane became more permeable. As the comparison of EDX data above indicates, the Pt concentration was far lower than in the Pt membranes. Accordingly, internal humidification and suppression of hydrogen permeation must have been significantly less. Consequently, the increase of $H_2$ flux can be linked to ionomer decomposition, resulting in a less dense membrane structure.

Electrical Conductivity. The electrical conductivity excludes by definition the influence of thickness and mainly reflects the proton transport in the membrane, since electric resistance and contact resistances are considered to be negligible. From the plot in Figure 18 the influence of the reduction step in the impregnation process becomes again apparent. The conductivity loss of 30 % of the Pt-MEA reduced with ethanol and at 60 °C exceeds significantly the values of the Pt-impregnated membranes reduced with 1-pentanol and at 120 °C. Compared to the data of FER and thickness loss, degradation in terms of conductivity is more pronounced. In contrast, the conductivity change of the other Pt-impregnated membranes varies between 6.0 and -4.5 % and displays no trend or correlation to other data. Most probably, this is the result of the contrary influence of increased water content due to self humidification and decomposition of the ionomer, which involves the proton conducting sulfonic groups. The greatest loss of conductivity with a value of 52 % exhibited the reference membrane. One reason was the precipitation of Pt, since its presence is decreasing conductivity as can be seen in Figure 12 for the Pt-

impregnated membranes. Furthermore, the loss of sulfonic groups certainly also diminished proton transport.

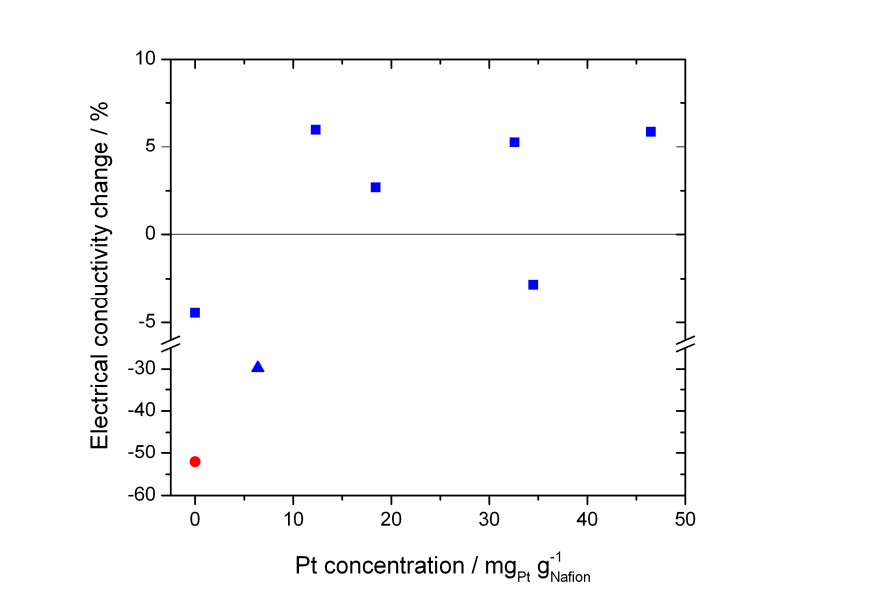


Figure 18. Change of electrical conductivity of the reference MEA (●), Pt-MEAs reduced with 1-pentanol at $T_{Pt, red}$ = 120 °C (■) and reduced with ethanol at $T_{Pt, red}$ = 60 °C (▲) during the degradation test.

## Conclusions

We investigated the influence of Pt precipitations and their concentration on the properties and degradation of the electrolyte membrane. Nafion® membranes impregnated with Pt showed that the increase in Pt concentration decreases the ionic conductivity of the membrane and increases the sensitivity of cell performance on humidification.

During the degradation test at OCV, membranes swelled due to reaction of $H_2$ and $O_2$ at the Pt deposit. As a consequence, water uptake influenced permeability and electrical conductivity, constricting their information value for degradation. The FER however, exhibited a correlation to size and distance of Pt precipitations. Ionomer decomposition was enhanced with an increase in concentration and surface area of Pt deposits as well as distance between particles.

The comparison with a non-impregnated membrane demonstrated that particle distribution of Pt precipitation forming during operation differed considerably from artificially precipitated Pt. Particles formed in-situ, were distributed more heterogeneously, in particular a Pt band is formed, and grew to a larger extent than in the Pt-impregnated membranes. Furthermore, they were less numerous and had a larger distance to each other. As a result, its total active surface area was lower. Besides, evidence for significant internal humidification and swelling was not observed. Probably because of this, ionomer degradation could not only be identified by means of FER, but also based on an increase of electrical resistance and $H_2$ permeability.

To confirm our data and assumptions, we will use additional analytical methods to determine more precisely Pt concentration and to examine the Pt-impregnated membranes for the presence of adsorbed water.

## Acknowledgement

The authors thank Marianne P. Rodgers for her helpful information and Steffen Wolf for the analysis of XRD data.

## References

1. A. B. LaConti, M. Hamdan, and R. C. McDonald, *Handbook of Fuel Cells: Fundamentals, Technology and Applications, Vol. 3.*, W. Vielstich, A. Lamm, and H. Gasteiger, Editors, vol. 3, p. 647–663, Chicester, England (2003).

2. J. Aragane, T. Murahashi, and T. Odaka, *J. Electrochem. Soc.*, **135**, 844–850 (1988).

3. J. Aragane, *J. Applied Electrochem,*, **26**, 147–152 (1996).

4. A. Ohma, S. Suga, S. Yamamoto, and K. Shinohara, *J. Electrochem. Soc.*, **154**, B757–760 (2007).

5. J. Zhang, B. A. Litteer, W. Gu, H. Liu, and H. A. Gasteiger, *J. Electrochem. Soc.*, **154**, B1006–1011 (2007).

6. J. Peron, Y. Nedellec, D. Jones, and J. Roziere, *J. Power Sources*, **185**, 1209–1217 (2008).

7. A. Ohma, S. Yamamoto, and K. Shinohara, *J. Power Sources*, **182**, 39–47 (2008).

8. W. Yoon and X. Huang, *J. Electrochem. Soc.*, **157**, B599 (2010).

9. T. Kim, H. Lee, W. Sim, Woojong, J. Lee, Jonghyun, S. Kim, Saehoon, T. Lim, Taewon, and K. Park, *Korean J. Chem. Eng.*, **26**, 1265–1271 (2010).

10. D. Zhao, B. L. Yi, H. M. Zhang, and M. Liu, *J. Power Sources*, **195**, 4606–4612 (2010).

11. N. Ohguri, A. Y. Nosaka, and Y. Nosaka, *J. Power Sources*, **195**, 4647–4652 (2010).

12. E. Endoh, S. Hommura, S. Terazono, H. Widjaja, and J. Anzai, *ECS Trans.*, **11**, 1083–1091 (2007).

13. M. Aoki, H. Uchida, and M. Watanabe, *ECS Trans.*, **3**, 485–492 (2006).

14. M. Gummalla, V. V. Atrazhev, D. Condit, N. Cipollini, T. Madden, N. Y. Kuzminyh, D. Weiss, and S. F. Burlatsky, *J. Electrochem. Soc.*, **157**, B1542–1548 (2010).

15. M. P. Rodgers, D. A. Cullen, J. Leonard, D. K. Slattery, and J. M. Fenton, in *Carisma 2012 - 3rd Carisma International Conference*, p. 1–19 (2012).

16. P. S. Fedkiw and W.-H. Her, *J. Electrochem. Soc.*, **136**, 899 (1989).

17. H. Hagihara, H. Uchida, and M. Watanabe, *Electrochi. Acta*, **51**, 3979–3985 (2006).

18. S. J. Sondheimer, N. J. Bunce, and C. A. Fyfe, *J. Macromol. Sci. , Part C*, **3**, 353–413 (1986).

19. E. Gülzow, M. Schulze, N. Wagner, T. Kaz, R. Reissner, G. Steinhilber and A. Schneider, *J. Power Sources*, **86**, 352–362 (2000).

20. X.-Z. Yuan, C. Song, H. Wang, and J. Zhang, *Electrochemical Impedance Spectroscopy in PEM Fuel Cells - Fundamentals and Applications*, Springer-Verlag London, London, (2010).

21. H. Liu, J. Zhang, F. D. Coms, W. Gu, B. Litteer and H. A. Gasteiger, *ECS Trans.*, **3**, 493–505 (2006).

22. R. Ahluwalia, S. Arisetty, R. Subbaraman, X. Wang, and D. Myers, in: 2nd International Workshop on Degradation Issues in Fuel Cells., Thessaloniki, Greece (2011) [Online], Available: http://iet.jrc.ec.europa.eu/fuel-cells/sites/fuel-cells/files/files/documents/events/dissolution_of_platinum_from_orr_catalysts_in_polymer_electrolyte_fuel_cells_-_r._ahluwalia.pdf (accessed 19 July 2013).

23. H.-K. Lee, J.-I. Kim, J.-H. Park, and T.-H. Lee, *Electrochim. Acta*, **50**, 761–768 (2004).

24. M. Watanabe, H. Uchida, Y. Seki, M. Emori, and P. Stoneheart, *J. Electrochem. Soc.*, **143**, 3847 (1996).

25. M. Inaba, T. Kinumoto, M. Kiriake, R. Umebayashi, A. Tasaka and Z. Ogumi, *Electrochim. Acta*, **51**, 5746–5753 (2006).